Target-Specific and Selective Drug Design for COVID-19 Using Deep Generative Models

Vijil Chenthamarakshan[1], Payel Das[*1], Inkit Padhi[1], Hendrik Strobelt[1],
Kar Wai Lim[2], Ben Hoover[1], Samuel C. Hoffman[1], and
Aleksandra Mojsilovic[1]

{ecvijil, daspa}@us.ibm.com, {inkpad, hendrik.strobelt}@ibm.com,
{kar.wai.lim, benjamin.hoover, shoffman}@ibm.com, aleksand@us.ibm.com

[1]IBM Research AI
[2]IBM Research Singapore

Abstract

The recent COVID-19 pandemic has highlighted the need for rapid therapeutic development for infectious diseases. To accelerate this process, we present a deep learning based generative modeling framework, CogMol, to design drug candidates specific to a given target protein sequence with high off-target selectivity. We augment this generative framework with an *in silico* screening process that accounts for toxicity, to lower the failure rate of the generated drug candidates in later stages of the drug development pipeline. We apply this framework to three relevant proteins of the SARS-CoV-2, the virus responsible for COVID-19, namely non-structural protein 9 (NSP9) replicase, main protease, and the receptor-binding domain (RBD) of the S protein. Docking to the target proteins demonstrate the potential of these generated molecules as ligands. Structural similarity analyses further imply novelty of the generated molecules with respect to the training dataset as well as possible biological association of a number of generated molecules that might be of relevance to COVID-19 therapeutic design. While the validation of these molecules is underway, we release ~ 3000 novel COVID-19 drug candidates generated using our framework.

1 Introduction

Generating novel drug molecules is a daunting task. The task aims at creating new molecules (or, optimize known molecules) with multiple desirable properties, that are often competing and tightly interacting with each other. For example, optimal drug molecules should be easy to synthesize, have binding affinity to a specific target protein

---

*Corresponding Author

1

of interest, low binding affinity to other targets, while also exhibiting high drug likeliness (QED). This makes drug discovery a costly (2-3 billion USD) and a time-consuming process (more than a decade) with a low success rate (less than 10%).

Traditional *in silico* molecule design and screening rely on considerable domain knowledge, physics-based simulations, and heuristic search algorithms. However, optimizing over the discrete, unstructured and sparse molecular space remains an intrinsically difficult challenge. As a result, there is a lot of interest in developing automated machine learning techniques to efficiently discover sizeable numbers of plausible, diverse and novel candidate molecules in the vast ($10^{23} - 10^{60}$) space of molecules [Polishchuk et al., 2013].

There has been a recent surge in the development of machine learning based models for candidate drug screening and novel molecule design. Simplified Molecular Input Line Entry Specification (SMILES), a text string representation of molecules, has been a popular choice for representing molecules in these models. Whereas earlier approaches to generate molecules involved recurrent neural networks (RNN) [Segler et al., 2017, Gupta et al., 2018], recent methods employ generative frameworks, such as the Variational Autoencoder (VAE) [Gómez-Bombarelli et al., 2018, Blaschke et al., 2018, Kang and Cho, 2018, Lim et al., 2018] and the Generative Adversarial Network (GAN)[Guimaraes et al., 2017].

There has recently been increasing interest in molecular graph-based generative methods [Li et al., 2018a, Li et al., 2018b, Simonovsky and Komodakis, 2018, Samanta et al., 2019, Ma et al., 2018, Kajino, 2018]. A particular challenge of SMILES-based generative approaches is to ensure that the generated strings are syntactically valid under SMILES grammar. [Kusner et al., 2017] and [Dai et al., 2018] added grammar constraints to SMILES strings to improve the chemical validity of the generated molecules. Unfortunately, this approach also suffers from several shortcomings. For example, the models are not permutation-invariant of their node labels, the training has a quadratic complexity concerning the number of nodes, and generating semantically valid graphs is challenging. [Jin et al., 2018] is considered as a state-of-the-art architecture in this context, which represents a molecular graph as fragments (such as rings and atom branches) connected in a tree structure. Among GAN-based approaches, [De Cao and Kipf, 2018] introduced MolGAN, a GAN trained with reinforcement learning (RL) for generating molecular graphs.

Reinforcement learning (RL) methods or Bayesian Optimization (BO) have often been employed on top of a SMILES-based or Graph-based molecule generator for ensuring valid molecule generation and/or generating molecules with a desired structure or property [Popova et al., 2018, Olivecrona et al., 2017, Jaques et al., 2017, Putin et al., 2018, Zhavoronkov et al., 2019, Gómez-Bombarelli et al., 2018]. Both BO [Gómez-Bombarelli et al., 2018] and RL [Zhou et al., 2019, Zhavoronkov et al., 2019] incur high computation cost, as they require a large number of evaluations. Semi-supervised learning has also been used for conditional generation [Lim et al., 2018, Kang and Cho, 2018, Li et al., 2018b], which needs labels to be available during generative model training.

In order to generate drugs that are specific to a particular target, the generative models in existing works [Zhavoronkov et al., 2019, Li et al., 2018b] are typically fine-tuned on the subset of molecules that bind with that target. This approach requires

model fine-tuning for a single target of interest and also limits the exploratory capability of the model in terms of generation. Accounting for off-target selectivity in a broader context also becomes non-trivial in this setting.

We propose an alternative method named **Co**ntrolled **G**eneration of **Mol**ecules — CogMol, that first learns a model capturing the vast molecular space using a variational autoencoder. We then map known relationships between protein sequences and existing drug molecules by training a binding affinity predictor posthoc on the learned latent features of drug molecules and protein sequence embeddings. The resulting model can handle candidate molecule generation for many target protein sequences, rather than requiring model retraining for every individual target. This approach also allows to perform controlled generation by explicitly taking off-target selectivity into account. Additional controls such as drug-likeliness can be added, to further finetune the controlled generation process.

Designed molecules are further screened using a multi-task deep learning classifier that was trained to predict toxicity on several *in vitro* and clinical endpoints. We hope that accounting for the important factors such as selectivity and toxicity within the AI framework will help the *in silico* drug design process to be faster, more agile, and less costly, leading to shorter discovery pipelines with high success rate.

Given the urgency with the ongoing COVID-19 pandemic, we apply CogMol to generate candidate molecules that bind to one of the three relevant target proteins of the SARS-CoV-2 virus, namely NSP9 Replicase, Main Protease, and the Receptor-Binding Domain (RBD) of the SARS-CoV-2 S protein, and act as their inhibitors (see Figure 1). The generated molecules might serve as a blueprint for creating drugs that can potentially bind to the viral protein with high target affinity, high off-target selectivity as well as high drug-likeliness.

```
> SARS-CoV-2 Main Protease
SGFRKMAFPSGKVEGCMVQVTCGTTTLNGLWLDDVVYCPRHVICTSEDMLNPNYEDLLIRKSNHNFLVQAGNVQLRVIGHSMQNCVLKLK
VDTANPKTPKYKFVRIQPGQTFSVLACYNGSPSGVYQCAMRPNFTIKGSFLNGSCGSVGFNIDYDCVSFCYMHHMELPTGVHAGTDLEGN
FYGPFVDRQTAQAAGTDTTITVNVLAWLYAAVINGDRWFLNRFTTTLNDFNLVAMKYNYEPLTQDHVDILGPLSAQTGIAVLDMCASLKE
LLQNGMNGRTILGSALLEDEFTPFDVVRQCSGVTFQ

> SARS-COV-2 NSP9 Replicase
SNAMNNELSPVALRQMSCAAGTTQTACTDDNALAYYNTTKGGRFVLALLSDLQDLKWARFPKSDGTGTIYTELEPPCRFVTDTPKGPKVK
YLYFIKGLNNLNRGMVLGSLAATVRLQ

> Receptor-Binding Domain (RBD) of SARS-COV-2 S protein
RVVPSGDVVRFPNITNLCPFGEVFNATKFPSVYAWERKKISNCVADYSVLYNSTFFSTFKCYGVSATKLNDLCFSNVYADSFVVKGDDVR
QIAPGQTGVIADYNYKLPDDFMGCVLAWNTRNIDATSTGNYNYKYRLFRKSNLKPFERDISTEIYQAGSTPCNGVEGFNCYFPLQSYGFQ
PTNGVGYQPYRVVVLSFELLNAPATVCGPKLSTDLIK
```

Figure 1: Sequences of SARS-CoV-2 targets

2   Molecule Generation Pipeline

As depicted in Figure 2, our target-specific drug design pipeline includes the following components:

- A Variational Autoencoder (VAE), first trained unsupervised and then jointly with attribute regressors (QED and Synthetic Accessibility, SA), that learns a disentangled latent space of the molecules on the SMILES representation.
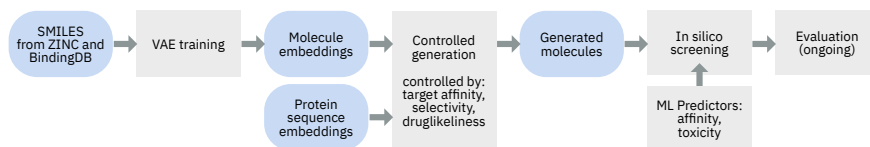
Figure 2: Workflow of the drug candidate generation pipeline

- A set of attribute regression models (predicting QED, off-target selectivity, and target affinity) trained on the VAE latent embeddings.

- An attribute-conditioned sampling scheme to generate molecules with desired attributes from the latent space.

- An *in silico* screening of generated molecules using sequence-level toxicity and affinity predictors.

The first three steps constitute CogMol and the last step empowers it with *in silico* screening.

3 Methods

3.1 Data

We used Moses benchmarking dataset [Polykovskiy et al., 2018] for the unsupervised VAE training, which include 250k/10k/10k molecules (training/test/scaffold test sets) from ZINC database [Irwin and Shoichet, 2005]. These molecules were filtered such that the molecular weight is in the range from 250 to 350 Daltons, the number of rotatable bonds is not greater than 7, and logP is less than or equal to 3.5. Molecules containing charged atoms as well as atoms besides C, N, S, O, F, Cl, Br, H or cycles longer than 8 atoms were removed. The molecules were further filtered via medicinal chemistry filters (MCFs) and PAINS filters.

For target-specific compound design, we used a curated IC50-labeled compound-protein binding data from BindingDB [Gilson et al., 2015], as reported in DeepAffinity [Karimi et al., 2018]. Since our objective is to build the best binding affinity (pIC50) regression model using available data, we also added the four excluded classes into our training data.

3.2 Variational Autoencoder for Molecule Generation

A Variational Autoencoder (VAE) [Kingma and Welling, 2013] frames an autoencoder in a probabilistic formalism that constrains the expressivity of the latent space, z. Each sample defines an encoding distribution $q_\phi(z|x)$ and for each sample, this encoder distribution is constrained to be close to a simple prior distribution $p(z)$. We consider the case of the encoder specifying a diagonal gaussian distribution only, i.e. $q_\phi(z|x) = N(z; \mu(x), \Sigma(x))$ with $\Sigma(x) = \text{diag}[\exp(\log(\sigma_d^2)(x)))]$.

Table 1: The performance metrics of the generative model: Fraction of valid molecules, Fraction of unique molecules from a sample of 1,000 and 10,000 molecules, Internal Diversity (IntDiv1 and IntDiv2), Fraction of molecules passing filters (MCF, PAINS, ring sizes, charges, atom types)

Model	Valid	Unique@1k	Unique@10k	IntDiv1	IntDiv2	Filters
ZINC (Unsupervised)	0.9553	1.0	0.9996	0.8568	0.8510	0.9889
ZINC (Supervised)	0.95	1.0	0.999	0.8578	0.8521	0.9888
BindingDB (Supervised)	0.904	1.0	0.9993	0.8717	0.8665	0.9482
CharRNN	0.809	1.0	1.0	0.855	0.849	0.975
AAE	0.997	1.0	0.995	0.857	0.85	0.997
VAE	0.969	1.0	0.999	0.856	0.851	0.996
JT-VAE	1.0	1.0	0.999	0.851	0.845	0.978
Training	1.0	1.0	1.0	0.857	0.851	1.0

The encoder neural network produces the log variances $\log(\sigma_d^2)(x)$. The marginal posterior is $q_\phi(\mathbf{z}) = \frac{1}{N} \sum_{j=1}^{N} q_\phi(\mathbf{z}|\mathbf{x}_j)$. The standard VAE objective is defined as follows (where D_{KL} is the Kullback-Leibler divergence),

$$\mathcal{L}_{\mathrm{VAE}}(\theta, \phi) = \mathbb{E}_{p(x)} \left\{ \mathbb{E}_{q_\phi(z|x)}[\log p_\theta(x|z)] - D_{\mathrm{KL}}(q_\phi(z|x)||p(z)) \right\}$$

We used a bidirectional Gated Recurrent Unit (GRU) with a linear output layer as an encoder. The decoder is a 3-layer GRU RNN of 512 hidden dimensions with intermediate dropout layers with dropout probability 0.2. Then, we jointly trained two property predictors, one for QED and one for SA, each parameterized by a feed-forward network, along with the VAE, to predict $y(x)$ from the latent embedding of x. Finally, we trained VAE with QED and SA predictors on BindingDB small molecules. We report the performance of the final VAE model in Table 1.

3.3 Latent Variable-based Predictors

To test the information content of the VAE latent space, we trained multiple attribute (QED, logP, and SA) predictors on the latent embeddings. These regression models have 4 hidden layers with 50 units each and ReLU nonlinearity. The performance of those predictors is reported in Table 2, showing low root-mean-square-error (RMSE) on test data for all three attribute predictors.

We also trained a binding affinity regression model using the IC50 data from BindingDB. This model takes a representation of a target protein sequence and latent embedding of a molecule as input and predicts the binding affinity between the protein-molecule pair. We used pretrained protein embeddings from [Bepler and Berger, 2019] to initialize the weights for proteins. The protein embedding and the molecular embedding are concatenated and passed through a single hidden layer with 2048 hidden units and ReLU nonlinearity. The best model with a test RMSE of 1.2310 was selected using extensive hyperparameter tuning (Table 2). We also trained a binding affinity predictor using SMILES ($\mathbf{x}$) instead of latent ($\mathbf{z}$) embedding as the input molecular representation, which yields an RMSE of 0.8426, comparable with recent work [Karimi et al., 2018].

5

Table 2: Performance of the attribute predictors for QED, logP, SA, and binding affinities. Binding affinity (z) is trained on the latent space of the VAE, while binding affinity (x) is trained on the actual SMILES sequences. Reported toxicity prediction result is an average over all Tox21 and ClinTox tasks.

Attribute	Metric	Our Method
QED	RMSE	0.0281
logP	RMSE	0.3307
SA	RMSE	0.0973
Binding Affinity (z)	RMSE	1.2310
Binding Affinity (x)	RMSE	0.8426
Toxicity Prediction	ROC AUC	0.7785
Toxicity Prediction	Precision	0.9389

3.4 Controlled Generation

Our objective is to generate molecules that simultaneously satisfy multiple (and often conflicting) objectives. Specifically, we want our generated molecules to have a high binding affinity to the selected SARS-CoV-2 target, high drug-likeliness, and high off-target selectivity.

Selectivity to a particular target is often modeled only in the later stages of a drug development pipeline and we believe that incorporating selectivity during the candidate generation stage will contribute to a reduction in the failure rate of drug candidates. We define selectivity as the excess binding affinity of a molecule to a target of interest over its average binding affinities to a random selection of k targets [Bosc et al., 2017].

$$Sel_{T,m} = BA(T,m) - \frac{1}{n}\sum_{i=1}^{k} BA(T_i,m)$$

We performed conditional sampling using Conditional Latent (attribute) Space Sampling — CLaSS, the method described in [Das et al., 2020]. In short, CLaSS leverages the attribute classifiers trained posthoc on the latent space and uses a rejection sampling scheme to generate samples with desired attributes. We added target binding affinity, off-target selectivity, and drug-likeliness as controls in the generation of candidate molecules. The distributions of CogMol-generated molecules in terms of binding affinity and off-target selectivity are displayed in Figure 3. Results indicate that generating high-affinity ligands is more challenging for NSP9 (Figure 3a), while Main Protease ligands are more selective (Figure 3b).

We show five randomly chosen samples from the top 1,000 generated molecules for each of the three SARS-CoV-2 targets in Figure 4.

3.5 *In Silico* Screening of Generated Molecules for Toxicity

Conventionally, molecular toxicity or side effect testing is carried out via different endpoint experiments such as *in vitro* molecular assays, *in vivo* animal testing, and clinical trials. However, these experiments are costly and time-consuming. Thus, as an
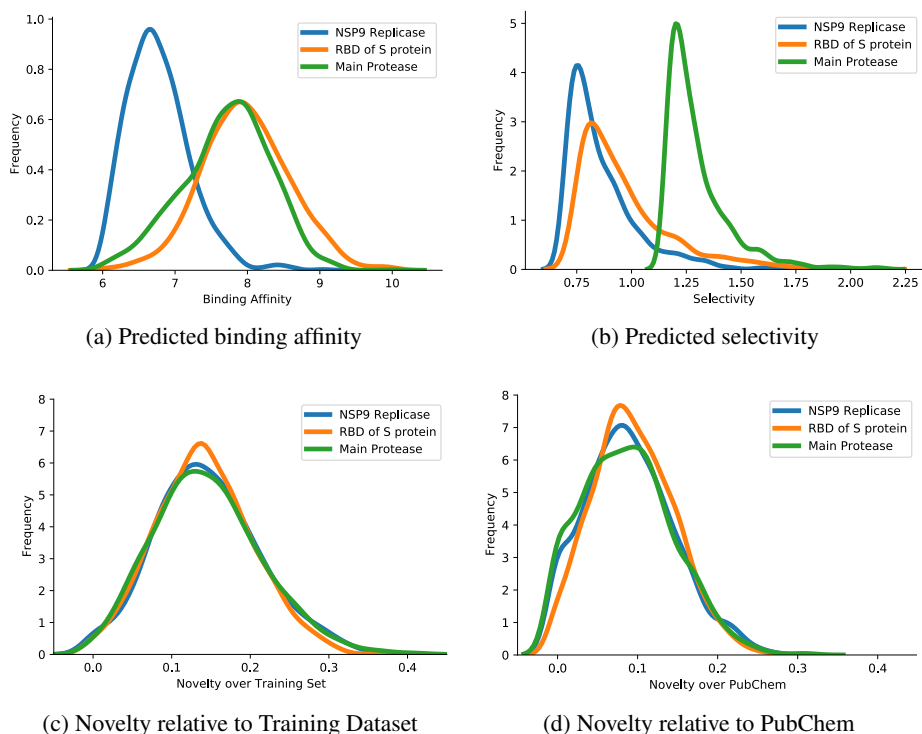
(a) Predicted binding affinity

(b) Predicted selectivity

(c) Novelty relative to Training Dataset

(d) Novelty relative to PubChem

Figure 3: Histograms of (a) binding affinity, (b) off-target selectivity, both predicted using **z** features, and (c-d) novelty (with respect to the training set and PubChem molecules) for the best 1,000 generated molecules.

in silico early screening tool, we used a multitask deep neural network (MT-DNN) to assess the toxicity of the molecules.

The MT-DNN was used to predict the toxicity on 12 *in vitro* endpoints as in the Tox21 challenge.[1] We also predicted whether the generated molecules would fail the clinical trials, using the ClinTox data [Wu et al., 2018]. This information allows us to prioritize the testing of molecules that are less likely to be harmful and can speed up the process of finding a COVID-19 therapeutic. We will continue to expand this model to include more endpoints.

Since a toxic substance is likely to exhibit toxicity across multiple endpoints, a multitask model can improve the prediction by exploiting the correlation between different endpoints. A multitask model is also more advantageous when the underlying training data is scarce (particularly in a clinical setting).

The MT-DNN model contains a total of four hidden layers: two are shared across all endpoints and two are private for each of the endpoints. We used a dropout [Srivastava et al., 2014] probability of 0.5, and a ReLU activation function for all layers except for the last layers, in which the sigmoid activation was used. Morgan Fingerprints [Rogers

---

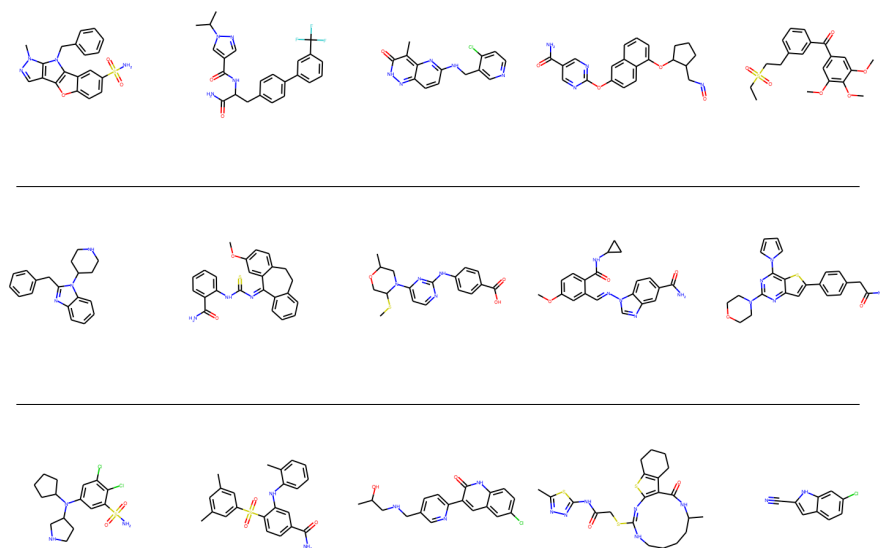[1]https://tripod.nih.gov/tox21/challenge/

Figure 4: Representative molecules generated for (top to bottom): NSP9 Replicase, Receptor-Binding Domain (RBD) of S protein, and Main Protease of SARS-CoV-2

and Hahn, 2010] were used as the input features to the model.

The ROC AUC, Accuracy (ACC), Balanced Accuracy (BAC), True Negative (TN), True Positive (TP), Precision (PR), Recall (RC), and the F1 score of the MT-DNN model on Tox21 and ClinTox test data are reported in Table 5 in the Appendix. Although the AUC values are slightly worse than the existing work of [Liu et al., 2019, see Table S14], the precision (and thus true positive rate) achieved by the MT-DNN is much higher.[2] For comparison, we also report the results from a random forest (RF) model in Table 6, showing that the MT-DNN significantly outperforms the RF model in terms of true positive rate, recall, and F1 score. Therefore, the MT-DNN model was used for assessing the generated molecules for toxicity. The molecule was considered toxic if it was predicted to be toxic in ≥ 2 endpoints.

We also screened the generated molecules for affinity and selectivity using the **x**-level binding affinity predictor (Table 2 and Sec 3.3), as the **x**-level affinity predictor yielded lower RMSE compared to the **z**-level one.

---

[2]The average precision from [Liu et al., 2019] over all 13 tasks is 0.45, which was obtained by running their code available through Github.

Table 3: Summary of Docking. For each target, multiple possible binding pockets were identified (Figure 7). For each of these binding pockets in a target, we calculated the binding free energies for all of the molecules specific to that target: average ($\pm$ standard deviation) over all generated molecules, minimum binding free energy in kcal/mol over all generated molecules, the fraction of generated molecules with binding free energy ≤ -6 kcal/mol. 88%, 94%, and 96% of generated molecules showed a binding free energy of ≤ -6 kcal/mol for at least one of the binding pockets in the specific target.

Target		Mean (kcal/mol)	Min (kcal/mol)	Low Energy (%)
NSP9 Dimer (88%)	pocket 1	-5.80 ± 0.65	-7.7	40
	pocket 2	-6.69 ± 0.75	-8.9	85
	pocket 3	-6.30 ± 0.74	-8.6	68
	pocket 4	-6.36 ± 0.69	-8.8	74
Main Protease (94%)	pocket 1	-7.13 ± 0.79	-9.5	93
	pocket 2	-6.68 ± 0.73	-9.4	83
	pocket 3	-6.24 ± 0.74	-8.5	66
	pocket 4	-6.36 ± 0.72	-8.6	72
RBD (96%)	pocket 1	-6.21 ± 0.63	-8.0	67
	pocket 2	-6.10 ± 0.57	-8.1	60
	pocket 3	-6.68 ± 0.62	-9.1	89
	pocket 4	-6.83 ± 0.65	-9.1	92
	pocket 5	-5.33 ± 0.53	-7.1	13
	pocket 6	-6.22 ± 0.64	-8.3	67

4   Analysis

4.1   Docking of Generated Molecules with Target Structure

To investigate the possible binding mode of the generated molecules with the target protein, we performed docking of the generated molecules against the potential binding sites (Figure 7) as predicted using PrankWeb [Krivák and Hoksza, 2018, Jendele et al., 2019] within the target structure using Autodock Vina [Trott and Olson, 2010]. Table 3 summarizes preliminary results from these docking runs. In the lowest energy docking mode, 88%, 94%, and 96% of generated molecules showed a binding free energy of ≤ -6 kcal/mol for at least one of the binding pockets in NSP9 dimer, Main Protease, and RBD, respectively. We also report the average and minimum binding free energy, as well as the fraction of generated molecules with a binding free energy of $\leq$ -6 kcal/mol for each pocket (Table 3). Figure 8 shows the best generated molecule (with lowest binding free energy) docked to a binding pocket in the target structure. These initial results imply the potential of these molecules as inhibitors for the COVID-19 targets, which will be further evaluated.

4.2   Novelty of Generated Molecules

To assess the novelty of generated molecules, we assigned to each molecule m a score Nov_m representing its minimal distance (maximal similarity) to all registered

Table 4: CogMol-generated SMILES that have reported biological activity in PubChem. For each target, predicted affinity from SMILES, lowest docking free energy (kcal/mol) with a specific pocket, pocket id shown in parenthesis, PubChem Compound ID (CID), and reported biological activity are reported.

Target	Pred. Affinity	Docking Energy	CID	Biological Activity
NSP9 Dimer	6.51	-7.60 (2)	12 042 753	Antagonist of rat mGluR
	7.06	-6.30 (1)	44 397 285	Active to human S6 kinase
	7.18	-6.30 (3)	10 570 770	Matrix metalloproteinase inhibitor
Main Protease	7.24	-6.30 (1)	10 608 757	Dihydrofolate reductase inhibitor
	6.91	-7.00 (1)	872 399	Shiga toxin inhibitor
RBD	7.82	-6.80 (1)	76 332 092	Plasmepsin inhibitor

compounds p in a reference database of known compounds P:

$$Nov_m = 1 - \max_{p \in P}\{\text{sim}(k_m, k_p)\}$$

To determine the similarity, we derive structural fingerprints, MACCS keys [Durant et al., 2002], for each pair of molecule (k_m) and compound (k_p). The Tanimoto [Willett et al., 1998] coefficient between two fingerprints expresses the similarity:

$$\text{sim}(k_x, k_y) = \frac{|k_x \cap k_y|}{|k_x \cup k_y|}$$

Note that a novelty of 0 means that the molecule's fingerprint matches exactly the fingerprint of a compound in the reference database.

The novelty distributions of the generated molecules with respect to both the Pubchem [Kim et al., 2018] database and our training set is given in Figure 3. The molecular fingerprints are further used to determine nearest neighbors within the generated molecules. Figure 5 shows an example of the most similar generated molecules (connected blue dots) of a selected generated molecule (in purple), that allows manual evaluation and filtering based on molecular diversity.

When compared with the training database of size $\sim$ 1.9 M, we find that the likelihood of generating molecules with a novelty value of 0 is $\leq$ 2%. With respect to the larger Pubchem database consisting of $\sim$ 103 M molecules, the majority of which were not included in model training, we find the percentage of generated molecules with novelty value of 0 is 9.5%, 3.7%, and 8.3% generated molecules for main protease, RBD, and NSP9, respectively. Only 19, 5, and 15 of them match exactly with an existing SMILES string in Pubchem.

As shown in Table 4, some of these SMILES are reported with *biological activity* in Pubchem, which calls for further investigation. For example, the molecule with Pubchem Compound ID (CID) 76332092 (labeled GEN_CRBD_146 in the data download) is a known Plasmepsin-2 and Plasmepsin-4 inhibitor. Plasmepsin family of proteins is a potential target for antimalarial drugs due to their haemoglobin-degrading activity.
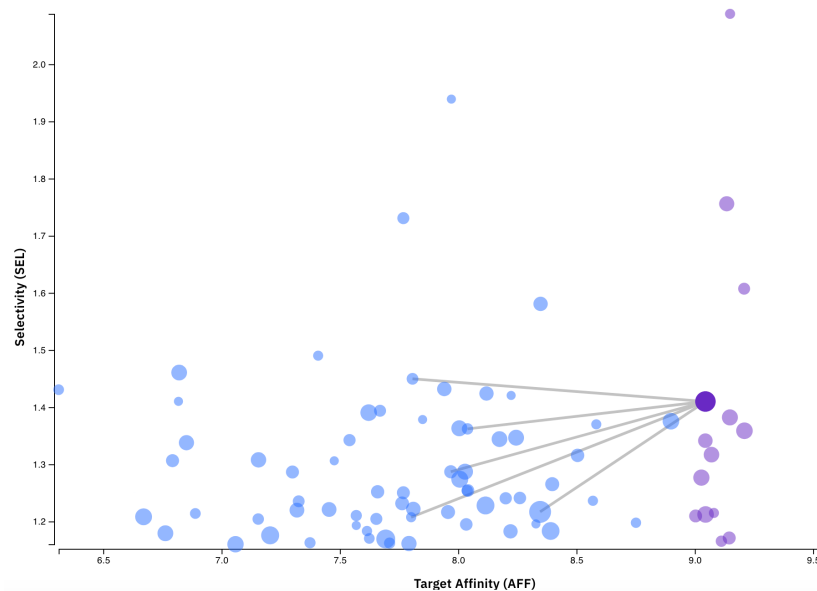
Figure 5: Neighborhood analysis: The top 15 molecules in terms of target affinity are shown in violet. For a selected top molecule, five structurally closest molecules are shown connected. Radius of the dot represents the novelty score (larger radius = more novelty) of the corresponding molecule.

CID 76332092 has also shown antimalarial activity against chloroquine-sensitive Plasmodium falciparum 3D7 infected in RBV after 72 hrs. Given that RBD from S protein binding to angiotensin-converting enzyme-2 (ACE-2) receptor is needed for viral entry to host cells [Hoffmann et al., 2020], both RBD and ACE-2 receptor are being actively investigated as COVID-19 targets. Chloroquine (and its hydroxy derivative) that is a known ACE-2 inhibitor has been already considered as a promising COVID-19 drug [Liu et al., 2020]. Given that chloroquine is also an anti-malaria drug, and that CID 76332092 shows a predicted pIC50 of 7.82 and lowest docking binding free energy of -6.80 kcal/mol (Figure 9) to the ACE-2 binding pocket of RBD (Table 4), this molecule deserves further investigation in the context of SARS-CoV-2. It is also noteworthy that the generated molecule with highest predicted pIC50 for RBD (and with docking binding free energy of -6.9 kcal/mol in the top binding mode with pocket 1) shares a strong maximum common subgraph similarity [Cao et al., 2008] with Telavancin, an approved Pneumonia drug, as shown in Figure 6. These results indicate that CogMol can generate promising and biologically relevant drug candidates beyond the training dataset.
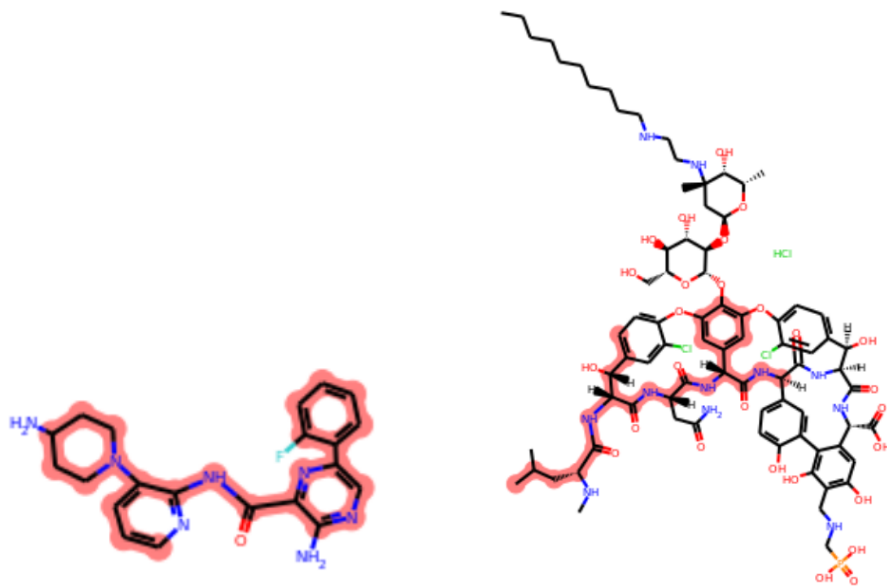
Figure 6: Maximum Common Subgraph Similarity of the CogMol-generated molecule with highest binding affinity to RBD (left) and Telavancin (right), a drug approved for nosocomial pneumonia.

5   Conclusions and Future Work

In this paper, we proposed CogMol, a framework for Controlled Generation of Molecules with a set of desired attributes. Our framework can handle candidate generations for multiple targets using the same trained model and also allows for explicit accounting of off-target selectivity. We also developed a method for screening generated candidates by using a model for predicting *in vitro* and clinical toxicity. Docking to the target protein shows the potential of these generated molecules as ligands. The novelty of the generated molecules was further investigated with respect to molecules in Pubchem. We expose 1,000 novel drug candidates for each of the three targets of the SARS-CoV-2 virus in the user interface.[3] Early structural analyses of the generated molecules reveal possible biological association that might be of relevance to COVID-19 therapeutic design. Validation of the generated promising molecules is underway and the paper will be updated with more results.

---

[3]https://covid19-mol.mybluemix.net/

References

[Bepler and Berger, 2019] Bepler, T. and Berger, B. (2019). Learning protein sequence embeddings using information from structure. In *International Conference on Learning Representations*, pages 1–17.

[Blaschke et al., 2018] Blaschke, T., Olivecrona, M., Engkvist, O., Bajorath, J., and Chen, H. (2018). Application of generative autoencoder in de novo molecular design. *Molecular Informatics*, 37(1-2):1700123.

[Bosc et al., 2017] Bosc, N., Meyer, C., and Bonnet, P. (2017). The use of novel selectivity metrics in kinase research. *BMC Bioinformatics*, 18(1):17.

[Cao et al., 2008] Cao, Y., Jiang, T., and Girke, T. (2008). A maximum common substructure-based algorithm for searching and predicting drug-like compounds. *Bioinformatics*, 24(13):i366–i374.

[Dai et al., 2018] Dai, H., Tian, Y., Dai, B., Skiena, S., and Song, L. (2018). Syntax-directed variational autoencoder for structured data. *arXiv preprint arXiv:1802.08786*.

[Das et al., 2020] Das, P., Sercu, T., Wadhawan, K., Padhi, I., Gehrmann, S., Cipcigan, F., Chenthamarakshan, V., Strobelt, H., dos Santos, C., Chen, P.-Y., Yang, Y. Y., Tan, J., Hedrick, J., Crain, J., and Mojsilovic, A. (2020). Accelerating antimicrobial design with controlled deep generative model and molecular simulation. *Under Review*.

[De Cao and Kipf, 2018] De Cao, N. and Kipf, T. (2018). MolGAN: An implicit generative model for small molecular graphs. *arXiv preprint arXiv:1805.11973*.

[Durant et al., 2002] Durant, J. L., Leland, B. A., Henry, D. R., and Nourse, J. G. (2002). Reoptimization of MDL keys for use in drug discovery. *Journal of Chemical Information and Computer Sciences*, 42(6):1273–1280.

[Gilson et al., 2015] Gilson, M. K., Liu, T., Baitaluk, M., Nicola, G., Hwang, L., and Chong, J. (2015). BindingDB in 2015: a public database for medicinal chemistry, computational chemistry and systems pharmacology. *Nucleic Acids Research*, 44(D1):D1045–D1053.

[Gómez-Bombarelli et al., 2018] Gómez-Bombarelli, R., Wei, J. N., Duvenaud, D., Hernández-Lobato, J. M., Sánchez-Lengeling, B., Sheberla, D., Aguilera-Iparraguirre, J., Hirzel, T. D., Adams, R. P., and Aspuru-Guzik, A. (2018). Automatic chemical design using a data-driven continuous representation of molecules. *ACS Central Science*, 4(2):268–276.

[Guimaraes et al., 2017] Guimaraes, G. L., Sanchez-Lengeling, B., Outeiral, C., Farias, P. L. C., and Aspuru-Guzik, A. (2017). Objective-reinforced generative adversarial networks (ORGAN) for sequence generation models. *arXiv preprint arXiv:1705.10843*.

[Gupta et al., 2018] Gupta, A., Müller, A. T., Huisman, B. J., Fuchs, J. A., Schneider, P., and Schneider, G. (2018). Generative recurrent networks for de novo drug design. *Molecular Informatics*, 37(1-2):1700111.

[Hoffmann et al., 2020] Hoffmann, M., Kleine-Weber, H., Schroeder, S., Krüger, N., Herrler, T., Erichsen, S., Schiergens, T. S., Herrler, G., Wu, N.-H., Nitsche, A., et al. (2020). SARS-CoV-2 cell entry depends on ACE2 and TMPRSS2 and is blocked by a clinically proven protease inhibitor. *Cell*.

[Irwin and Shoichet, 2005] Irwin, J. J. and Shoichet, B. K. (2005). ZINC–a free database of commercially available compounds for virtual screening. *Journal of Chemical Information and Modeling*, 45(1):177–182.

[Jaques et al., 2017] Jaques, N., Gu, S., Bahdanau, D., Hernández-Lobato, J. M., Turner, R. E., and Eck, D. (2017). Sequence tutor: Conservative fine-tuning of sequence generation models with KL-control. In *Proceedings of the 34th International Conference on Machine Learning*, pages 1645–1654. JMLR.org.

[Jendele et al., 2019] Jendele, L., Krivak, R., Skoda, P., Novotny, M., and Hoksza, D. (2019). PrankWeb: a web server for ligand binding site prediction and visualization. *Nucleic Acids Research*, 47(W1):W345–W349.

[Jin et al., 2018] Jin, W., Barzilay, R., and Jaakkola, T. (2018). Junction tree variational autoencoder for molecular graph generation. *arXiv preprint arXiv:1802.04364*.

[Kajino, 2018] Kajino, H. (2018). Molecular hypergraph grammar with its application to molecular optimization. *arXiv preprint arXiv:1809.02745*.

[Kang and Cho, 2018] Kang, S. and Cho, K. (2018). Conditional molecular design with deep generative models. *Journal of Chemical Information and Modeling*, 59(1):43–52.

[Karimi et al., 2018] Karimi, M., Wu, D., Wang, Z., and Shen, Y. (2018). DeepAffinity: interpretable deep learning of compound-protein affinity through unified recurrent and convolutional neural networks. *arXiv preprint arXiv:1806.07537*.

[Kim et al., 2018] Kim, S., Chen, J., Cheng, T., Gindulyte, A., He, J., He, S., Li, Q., Shoemaker, B. A., Thiessen, P. A., Yu, B., Zaslavsky, L., Zhang, J., and Bolton, E. E. (2018). PubChem 2019 update: improved access to chemical data. *Nucleic Acids Research*, 47(D1):D1102–D1109.

[Kingma and Welling, 2013] Kingma, D. P. and Welling, M. (2013). Auto-encoding variational Bayes. *arXiv preprint arXiv:1312.6114*.

[Krivák and Hoksza, 2018] Krivák, R. and Hoksza, D. (2018). P2Rank: machine learning based tool for rapid and accurate prediction of ligand binding sites from protein structure. *Journal of Cheminformatics*, 10(1):39.

[Kusner et al., 2017] Kusner, M. J., Paige, B., and Hernández-Lobato, J. M. (2017). Grammar variational autoencoder. In *Proceedings of the 34th International Conference on Machine Learning*, pages 1945–1954. JMLR.org.

[Li et al., 2018a] Li, Y., Vinyals, O., Dyer, C., Pascanu, R., and Battaglia, P. (2018a). Learning deep generative models of graphs. *arXiv preprint arXiv:1803.03324*.

[Li et al., 2018b] Li, Y., Zhang, L., and Liu, Z. (2018b). Multi-objective de novo drug design with conditional graph generative model. *Journal of Cheminformatics*, 10(1):33.

[Lim et al., 2018] Lim, J., Ryu, S., Kim, J. W., and Kim, W. Y. (2018). Molecular generative model based on conditional variational autoencoder for de novo molecular design. *Journal of Cheminformatics*, 10(1):31.

[Liu et al., 2020] Liu, J., Cao, R., Xu, M., Wang, X., Zhang, H., Hu, H., Li, Y., Hu, Z., Zhong, W., and Wang, M. (2020). Hydroxychloroquine, a less toxic derivative of chloroquine, is effective in inhibiting SARS-CoV-2 infection in vitro. *Cell Discovery*, 6(1):1–4.

[Liu et al., 2019] Liu, S., Demirel, M. F., and Liang, Y. (2019). N-gram graph: Simple unsupervised representation for graphs, with applications to molecules. In *Advances in Neural Information Processing Systems*, pages 8464–8476.

[Ma et al., 2018] Ma, T., Chen, J., and Xiao, C. (2018). Constrained generation of semantically valid graphs via regularizing variational autoencoders. In *Advances in Neural Information Processing Systems*, pages 7113–7124.

[Olivecrona et al., 2017] Olivecrona, M., Blaschke, T., Engkvist, O., and Chen, H. (2017). Molecular de-novo design through deep reinforcement learning. *Journal of Cheminformatics*, 9(1):48.

[Polishchuk et al., 2013] Polishchuk, P. G., Madzhidov, T. I., and Varnek, A. (2013). Estimation of the size of drug-like chemical space based on GDB-17 data. *Journal of Computer-Aided Molecular Design*, 27(8):675–679.

[Polykovskiy et al., 2018] Polykovskiy, D., Zhebrak, A., Sanchez-Lengeling, B., Golovanov, S., Tatanov, O., Belyaev, S., Kurbanov, R., Artamonov, A., Aladinskiy, V., Veselov, M., Kadurin, A., Nikolenko, S., Aspuru-Guzik, A., and Zhavoronkov, A. (2018). Molecular sets (MOSES): A benchmarking platform for molecular generation models. *arXiv preprint arXiv:1811.12823*.

[Popova et al., 2018] Popova, M., Isayev, O., and Tropsha, A. (2018). Deep reinforcement learning for de novo drug design. *Science Advances*, 4(7):eaap7885.

[Putin et al., 2018] Putin, E., Asadulaev, A., Ivanenkov, Y., Aladinskiy, V., Sanchez-Lengeling, B., Aspuru-Guzik, A., and Zhavoronkov, A. (2018). Reinforced adversarial neural computer for de novo molecular design. *Journal of Chemical Information and Modeling*, 58(6):1194–1204.

[Rogers and Hahn, 2010] Rogers, D. and Hahn, M. (2010). Extended-connectivity fingerprints. *Journal of Chemical Information and Modeling*, 50(5):742–754.

[Samanta et al., 2019] Samanta, B., Abir, D., Jana, G., Chattaraj, P. K., Ganguly, N., and Rodriguez, M. G. (2019). NeVAE: a deep generative model for molecular graphs. In *Proceedings of the AAAI Conference on Artificial Intelligence*, volume 33, pages 1110–1117.

[Segler et al., 2017] Segler, M. H., Kogej, T., Tyrchan, C., and Waller, M. P. (2017). Generating focused molecule libraries for drug discovery with recurrent neural networks. *ACS Central Science*, 4(1):120–131.

[Simonovsky and Komodakis, 2018] Simonovsky, M. and Komodakis, N. (2018). GraphVAE: Towards generation of small graphs using variational autoencoders. In *International Conference on Artificial Neural Networks*, pages 412–422. Springer.

[Srivastava et al., 2014] Srivastava, N., Hinton, G., Krizhevsky, A., Sutskever, I., and Salakhutdinov, R. (2014). Dropout: a simple way to prevent neural networks from overfitting. *The Journal of Machine Learning Research*, 15(1):1929–1958.

[Trott and Olson, 2010] Trott, O. and Olson, A. J. (2010). AutoDock Vina: improving the speed and accuracy of docking with a new scoring function, efficient optimization, and multithreading. *Journal of Computational Chemistry*, 31(2):455–461.

[Willett et al., 1998] Willett, P., Barnard, J. M., and Downs, G. M. (1998). Chemical similarity searching. *Journal of Chemical Information and Computer Sciences*, 38(6):983–996.

[Wu et al., 2018] Wu, Z., Ramsundar, B., Feinberg, E. N., Gomes, J., Geniesse, C., Pappu, A. S., Leswing, K., and Pande, V. (2018). MoleculeNet: a benchmark for molecular machine learning. *Chemical Science*, 9(2):513–530.

[Zhavoronkov et al., 2019] Zhavoronkov, A., Ivanenkov, Y. A., Aliper, A., Veselov, M. S., Aladinskiy, V. A., Aladinskaya, A. V., . Terentiev, V. A., Polykovskiy, D. A., Kuznetsov, M. D., Asadulaev, A., Volkov, Y., Zholus, A., Shayakhmetov, R. R., Zhebrak, A., Minaeva, L. I., Zagribelnyy, B. A., Lee, L. H., Soll, R., Madge, D., Xing, L., Tao, G., and Aspuru-Guzik, A. (2019). Deep learning enables rapid identification of potent DDR1 kinase inhibitors. *Nature Biotechnology*, 37:1038—1040.

[Zhou et al., 2019] Zhou, Z., Kearnes, S., Li, L., Zare, R. N., and Riley, P. (2019). Optimization of molecules via deep reinforcement learning. *Scientific Reports*, 9(1):10752.

A Performance of MT-DNN Toxicity Predictor

Tables 5 and 6 show the performance of toxicity prediction using the MT-DNN and the random forest as the baseline. The MT-DNN significantly outperforms the RF model in terms of true positive rate, recall, and F1 score, while incurring a small penalty in ROC AUC and precision.

Table 5: Performance on toxicity prediction using MT-DNN for all 12 Tox21 tasks and ClinTox task (CT-TOX). The reported metrics are ROC AUC, accuracy, balanced accuracy, true negative rate, true positive rate, precision, recall, and the F1 score. Refer to Table 6 for a comparison with random forest, the MT-DNN achieves much better true positive, recall and F1 score with slight penalty on AUC.

Task	AUC	ACC	BAC	TN	TP	PR	RC	F1
NR-AR	0.72	0.97	0.73	0.99	0.46	0.98	0.46	0.55
NR-Aromatase	0.78	0.95	0.65	0.99	0.31	0.96	0.31	0.41
NR-PPAR-γ	0.75	0.97	0.61	0.99	0.23	0.96	0.23	0.31
SR-HSE	0.75	0.94	0.61	0.99	0.23	0.94	0.23	0.32
NR-AR-LBD	0.82	0.98	0.78	0.99	0.56	0.99	0.56	0.66
NR-ER	0.69	0.88	0.64	0.96	0.32	0.89	0.32	0.40
SR-ARE	0.78	0.86	0.67	0.95	0.39	0.88	0.39	0.47
SR-MMP	0.87	0.89	0.75	0.96	0.54	0.93	0.54	0.62
NR-AhR	0.85	0.91	0.73	0.96	0.50	0.93	0.50	0.55
NR-ER-LBD	0.78	0.96	0.69	0.99	0.38	0.97	0.38	0.48
SR-ATAD5	0.75	0.96	0.61	0.99	0.22	0.97	0.22	0.32
SR-p53	0.79	0.94	0.64	0.99	0.29	0.96	0.29	0.40
CT-TOX	0.79	0.92	0.61	0.97	0.25	0.84	0.25	0.31
Average	0.78	0.93	**0.67**	0.98	**0.36**	0.94	**0.36**	**0.45**

Table 6: Performance on toxicity prediction for Random Forest on all 12 Tox21 tasks and ClinTox task (CT-TOX). The reported metrics are ROC AUC, accuracy, balanced accuracy, true negative rate, true positive rate, precision, recall, and the F1 score.

| Task	AUC	ACC	BAC	TN	TP	PR	RC	F1
NR-AR	0.78	0.98	0.73	0.99	0.46	0.99	0.46	0.60
NR-Aromatase	0.81	0.96	0.60	0.99	0.21	0.98	0.21	0.32
NR-PPAR-gamma	0.82	0.97	0.56	0.99	0.12	0.99	0.12	0.20
SR-HSE	0.77	0.95	0.56	0.99	0.13	0.97	0.13	0.22
NR-AR-LBD	0.85	0.98	0.77	0.99	0.54	0.99	0.54	0.66
NR-ER	0.72	0.89	0.60	0.98	0.21	0.93	0.21	0.32
SR-ARE	0.81	0.86	0.61	0.99	0.24	0.94	0.24	0.36
SR-MMP	0.88	0.89	0.67	0.98	0.36	0.95	0.36	0.49
NR-AhR	0.89	0.91	0.65	0.99	0.32	0.96	0.32	0.45
NR-ER-LBD	0.80	0.96	0.65	0.99	0.31	0.99	0.31	0.45
SR-ATAD5	0.84	0.96	0.55	0.99	0.10	0.97	0.10	0.18
SR-p53	0.83	0.95	0.56	0.99	0.13	0.99	0.13	0.22
CT-TOX	0.76	0.92	0.55	0.98	0.13	0.85	0.13	0.19
Average	**0.81**	0.94	0.62	0.99	0.25	0.96	0.25	0.36

# B   Additional Results: Docking
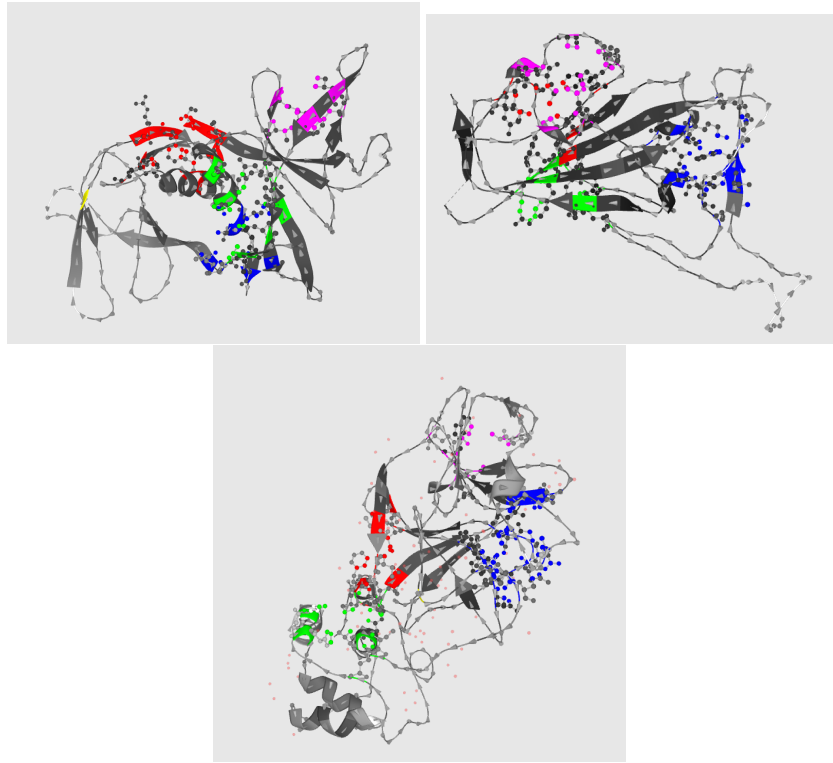
Figure 7: Binding pockets predicted using PrankWeb [Krivák and Hoksza, 2018, Jendele et al., 2019] for NSP9 Replicase (left), receptor-Binding Domain (RBD) of S protein (right), and Main Protease (bottom) of SARS-CoV-2. The binding pockets are colored according to the score (a combination of predicted ligandability and conservation) in this order: blue>green>red>purple>white. Pockets are indexed $1....n$ according to their score. These indexes are used to refer to a specific pocket throughout this study.
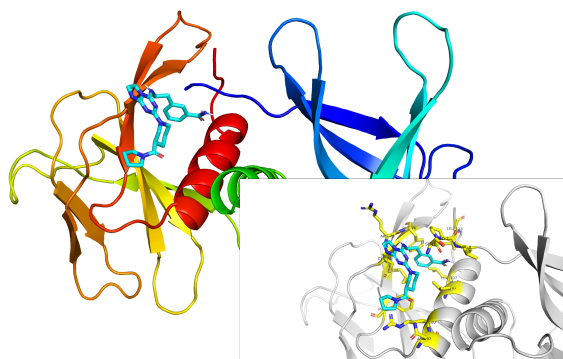
(a) NSP9 Dimer (pocket 1)
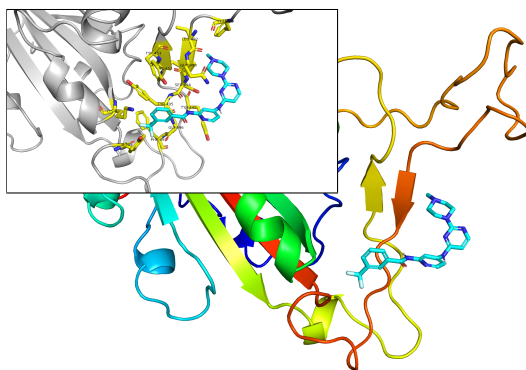
(b) RBD (pocket 1)
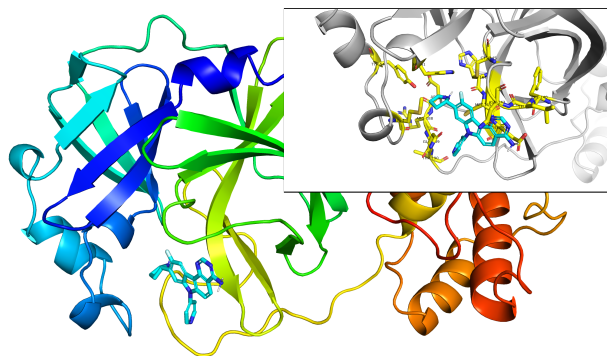
(c) Main Protease (pocket 1)

Figure 8: Predicted lowest energy binding mode for top generated molecule (in terms of docking binding free energy) with the corresponding target. Inset is a zoomed view showing the protein residues (within 4 angstroms) of the generated ligand.
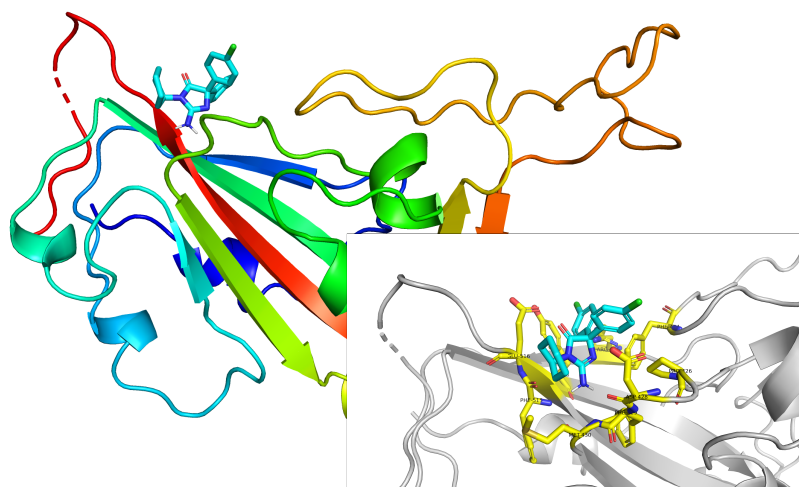
Figure 9: Predicted lowest energy binding mode for Pubchem Compound ID 76332092 with RBD.